Thermoluminescence and Radioluminescence of alexandrite mineral

Neilo Marcos Trindade*[1,2], Marcela Rodrigues da Cruz[3], Henrique Kahn[4], Luiz Gustavo Jacobsohn[2], Elisabeth Mateus Yoshimura[3].

[1] Department of Physics, Federal Institute of Education, Science and Technology of São Paulo - IFSP, São Paulo, SP, Brazil.

[2] Department of Materials Science and Engineering, Clemson University, Clemson, SC, USA.

[3] Institute of Physics, University of São Paulo - USP, São Paulo, SP, Brazil.

[4] Polytechnic School, University of São Paulo - USP, São Paulo, SP, Brazil

*ntrindade@ifsp.edu.br (N. M. Trindade); marcela.rodrigues.cruz@usp.br (M. R. Cruz); henrique@lct.poli.usp.br (H. Kahn); luiz@clemson.edu (L. G. Jacobsohn); e.yoshimura@if.usp.br (E. M. Yoshimura).

ABSTRACT

The thermoluminescence (TL) of natural alexandrite ($BeAl_2O_4$) was investigated using different methods, namely T_m-T_{stop}, T_m as a function of beta irradiation dose, glow curve best fitting, variable heating rate, and TL fading as a function of time after irradiation, in addition to radioluminescence (RL) measurements under X-ray excitation as a function of the temperature. The chemical composition and the concentration of secondary mineral phases were determined by scanning electron microscopy and Energy-dispersive X-ray spectroscopy. TL measurements with heating rate = 1 K/s revealed five individual TL peaks at about 355 (peak I), 405 (peak II), 435 (peak III), 530 (peak IV), and 580 K (peak V). The activation energy *E* and the frequency factor *s* associated with each of them were determined by different methods. Within irradiation doses from 1 to 10 Gy, analysis of the T_m position indicated that all glow peaks exhibited a first-order kinetics TL mechanism. TL fading at room temperature was 15% for peak IV and 5% for peak V within 2 days after irradiation. RL measurements revealed luminescence centers attributed to Cr^{3+}, Mn^{4+} and Fe^{3+} impurities. Overall, the results suggest that natural alexandrite has a potential use in dosimetry.

Keywords: alexandrite, thermoluminescence, glow curve, natural dosimeter.

1. INTRODUTION

Alexandrite is a green variety of chrysoberyl with the incorporation of chromium in its lattice [1, 2]. Chrysoberyl is one of the most interesting minerals with wide application in lasers being widely used for medical purposes, since it exhibits higher performance of the laser than other materials[3]. Chrysoberyl ($BeAl_2O_4$) has orthorhombic symmetry (*Pmna*) that corresponds to a hexagonal-close-packed in which the position of the oxygen atoms is slightly distorted [4]. These distortions give rise to two crystallographic sites with different symmetries: the site Al_1 corresponds to an inversion center (Ci symmetry), and the site Al_2 is located in a reflection plane (Cs symmetry) [5-7]. Chromium (Cr^{3+}) and Iron (Fe^{3+}) as impurities are often responsible for the optical properties of this mineral [3]. When doped, the Cr^{3+} ions preferably replace about 75% on the site Al_2 and 25% on the Al_1 site [2, 8-12]. When with the presence of iron, Fe^{3+} substitutes in different Al^{2+} octahedral sites with the proportion of 60% on the Al_1 and 40% on Al_2 site [3].

Noteworthy, Brazil is one of the largest world producers of alexandrite and in spite of belonging to a family of gems with economic and technological interest [13], there are few studies on the applications of natural alexandrite. Furthermore, the fact that chrysoberyl contains around of 20 wt.% BeO and 80 wt.% Al_2O_3 [6], and that both of these oxides are commercially used as dosimeters [14, 15], suggested the investigation of alexandrite as a natural dosimeter [16], through the use of thermoluminescence technique.

Thermoluminescence (TL) is the light emitted by some materials upon heating after exposure to ionizing radiation, besides incandescence. It is a thermally stimulated emission originated in the release of charge carriers from traps and their recombination at luminescence centers [17, 18]. Among the thermoluminescent materials, some natural

minerals can be used for TL dosimetry [19], nuclear accident dosimetry [20], food irradiation control [21], and luminescence dating [22]. Among them, quartz [23-26], calcite [27, 28] and feldspar [22, 29] are well-known thermoluminescent minerals, and recently we showed that the mineral alexandrite has potential for use in dosimetry [16]. In addition, to complement TL experimental technique, Radioluminescence (RL) is used as an important tool for studying luminescence mechanisms. RL is the luminescence emitted by a material under exposure to ionizing radiation. This technique provides emission energy information as a function of sample temperature, which in general are related to impurities or dopants in the material [30]. To the best of our knowledge, there is only one report on the investigation of the effects of ionizing radiation on synthetic alexandrite [31], two reports on the TL response of natural alexandrite and chrysoberyl [16, 32] and we have no notice about any work of radioluminescence measures in alexandrite.

The objectives of this work were the investigation of the TL behavior and of the recombination centers by means of RL measurements of alexandrite. In this work, kinetic behavior of the TL glow peaks of alexandrite through the determination of the activation energy, *E*, and frequency factor, *s*, of each TL peak as well as RL results are reported for the first time.

2. MATERIALS AND METHODS

Two samples were extracted from the same rock of natural alexandrite originated from the State of Bahia, Brazil. Both samples were sliced with parallel faces, thickness of 1.0 mm, and masses of 0.059 ± 0.001g (sample I) and 0.045± 0.001g (sample II). During sample handling, sample I broke into several fragments (Fig. 1a).

Chemical analysis and imaging were carried out by means of scanning electron microscopy (SEM)/electron dispersive X-ray spectroscopy (EDS) measurements on all fragments of sample I (Fig. 1b). The fragments were mounted onto a 30 mm diameter epoxy resin block (Epofix–Struers) and polished with diamond. For these measurements, a LEO Stereoscan 440 scanning electron microscope operated at an accelerating voltage of 20 kV and equipped with an Oxford x-act EDS spectrometer was used. Backscattered electron (BSE) imaging was used to complement EDS chemical characterization. Standards from Smithsonian Institute and Micro-Analysis Cons. Ltd. were used in the EDS analysis. As Be concentration is not possible to evaluate by EDS, we assumed the presence of this element in a concentration corresponding to BeO in the sample, completing the set of oxides (Al_2O_3, Cr_2O_3 and Fe_2O_3) in the matrix, stoichiometrically. Chemical compositions of allanite, apatite and fluorite were also fine-tuned according to the atomic proportions of the bearing elements which is not possible to do in relation to micas due the presence of light elements not analyzed by EDS.

TL measurements were executed on sample I. For these measurements, the sample was heated at 20 K/min up to 773 K in a muffle furnace and kept at this temperature for 1h to empty the traps and erase the effects of previous irradiations. The sample was then cooled at 20 K/min up to room temperature. TL measurements were carried out using a commercial automated TL/OSL reader fabricated by Risø National Laboratory (model DA-20). TL glow curves were obtained using a heating rate of 1 K/s, from room temperature to 723 K. The TL signal was detected with a bialkali photomultiplier tube behind an UV transmitting filter (Hoya U-340, 7.5 mm thick) and a 5 mm dia. mask. Irradiations were performed at room temperature using the built-in $^{90}Sr/^{90}Y$ beta source of the TL/OSL reader (dose rate of 10 mGy/s).

The analysis of the glow curves and the extraction of the kinetic parameters involved several methods, including T_m-T_{stop}, T_m as a function of irradiation dose (dose range from 1 to 10 Gy), variable heating rate (β from 0.4 to 5 K/s), and glow curve fitting. These methods have been established and discussed in [17, 33, 34]. The protocol used for the T_m-T_{stop} method was as follows:

1. Irradiation of the sample up to 1 Gy
2. Sample heating at a constant rate (β = 1 K/s) up to a T_{stop} temperature
3. Sample cooling down to room temperature
4. Acquisition of a full TL glow curve, from RT to 668 K, and determination of the temperature, T_m, of the peak that was closest to T_{stop}

This sequence was repeated several times, increasing T_{stop} by 5 K from 333 K up to 668 K, thus completing the whole TL curve. Glow curve analysis used the GlowFit software [35] that is based on the first-order kinetics model by Randall-Wilkins [36]. Further, an investigation of the immediate fading of the TL signal was conducted with the sample beta-irradiated and stored in the dark at room temperature for various times up to 48 h before the TL readout.

RL measurements were executed on sample II using a customer-designed Freiberg Instruments Lexsyg Research spectrofluorometer equipped with a Varian Medical Systems VF-50J X-ray tube with a tungsten target and coupled with an ionization chamber for dose monitoring. The light emitted by the sample was collected by a lens and converged into an optical fiber connected to an Andor Technology Shamrock 163 spectrograph coupled to an Andor Technology DU920P-BU Newton CCD camera. Results were not corrected for the spectral sensitivity of the system. RL measurements were executed under continuous X-ray irradiation (40 kV and 1 mA) from RT up to 673 K with a heating rate of 1 K/s and 1 s integration time. The measurements were done in

150 steps of 50 K, keeping the sample at the chosen temperature for 5 s before beginning the
151 data collection to guarantee thermal stability.
152
153 ## 3. RESULTS AND DISCUSSION
154 Fig. 1a illustrates the visual aspect of the fragments of sample I where the presence of
155 different mineral phases can be seen. Fig. 1b shows a typical BSE image of the same
156 fragments. The differences between the many shades of grey revealed variations of the
157 chemical composition and confirmed the existence of several mineral phases, as detailed
158 in the legend (upper part of Fig. 1b). The presence of various mineral phases is expected
159 in a natural sample. Figs. 1c and 1d show BSE images of the fragment with the highest
160 fraction of alexandrite at different magnifications illustrating the natural distribution of
161 the mineral phases within the fragment. The proportion of the mineral phases among all
162 the fragments was determined by image analyze considering phase contrast on
163 backscattered electron (BSE) image and chemical compositions by EDS analysis; area
164 proportions were converted to weight considering average mineral specific gravity to be
165 62 wt.% alexandrite, 22 wt.% apatite – calcium phosphate, 13 wt.% mica, 3 wt.%
166 calcium aluminosilicate with rare earths – allanite, and traces of fluorite.
167 The determination of the chemical composition was important in order to
168 understand the luminescent behavior and to allow for future correlation between these
169 results and results from other minerals. Table I shows the average weight percentages of
170 the binary oxides and halides that compose each mineral phase of all the fragments of
171 sample I. The determination of the presence of Cr and Fe in alexandrite is important
172 because it influences the optical and electrical properties related of the material [37, 38].
173 Figure 2 shows a typical glow curve of alexandrite measured at 1 K/s after
174 irradiation up to 1 Gy. Five peaks labeled I (~355 K), II (~405 K), III (~435K), IV

(~530 K), and V (~580 K) were observed. The nature of these peaks was investigated by the T_m-T_{stop} method. The constancy of T_m with the increase of T_{stop} is expected for a first-order kinetics TL peak, while a shift toward higher temperatures characterizes a non-first order kinetics TL peak [17, 39]. Accordingly, Fig. 3 shows that peaks I, II, IV and V present first-order kinetics. On the other hand, the results for peak III presented a higher level of uncertainty because of its weaker relative intensity combined with its proximity to peaks II and IV and no clear conclusion could be drawn. The nature of this TL peak is further discussed below.

The analysis of T_m as a function of the irradiation dose was also executed. For a first-order kinetics TL peak, the peak position is not expected to change as a function of the irradiation dose [17, 39]. Fig. 4 shows the glow curves obtained for different irradiation doses, from 1 to 10 Gy, while the inset shows the T_m values extracted directly from the glow curve and through the use of the GlowFit software. Both T_m analyzes (Fig. 4, inset) showed essentially the same behavior in which the peak positions were independent of the dose, including peak III, thus corroborating and expanding the T_m-T_{stop} results in that all the TL peaks presented a first-order kinetics TL mechanism. Fig. 5 shows the best fitting obtained with GlowFit (continuous green lines) of the experimental glow curves (continuous black lines). For each glow curve, five TL peaks (dashed red lines) were considered as per the results obtained with the T_m-T_{stop} analysis and the figure of merit (FOM) describing the quality of the fitting is given for each plot. All fittings had a FOM below 5%, and non-biased residuals, demonstrating the good quality of the fitting.

GlowFit also yielded the peak intensity, integral area, trap depth energy E, and frequency factor s of each fitted peak. The dose response curves based on the peak intensity and area values are shown in Fig. 6. The dose response curves of all five peaks

showed a linear increase with dose. In addition, Fig. 7 shows the *E* values as a function of the irradiation dose for each peak. Besides peak I, all other peaks yielded an essentially constant *E* value for all irradiation doses. The behavior of peak I that is centered at 355 K (β = 1 K/s) is tentatively explained by some difficulty of the *Glow Fit* software in dealing with two low-intensity peaks with so close *E* values, as are peaks I and II. Nevertheless, the average *E* values and the *s* values together with their respective standard deviations for both methods are presented in Table II.

The *E* and *s* values were also obtained using the variable heating rate method [17, 18, 33]. Fig. 8 shows the glow curves obtained at various heating rates where a shift of T_m toward higher values for faster heating rates was observed. The behavior of peaks IV and V at the higher heating rates points to a possible thermal quenching effect, as the peak intensities have a marked decrease compared to the rest of the glow curve. According to the equation $\frac{\beta \cdot E}{k \cdot T_m^2} = s\, exp\{-E/kT_m\}$ [17], the plot of $ln(T_m^2/\beta)$ against $1/kT_m$ (k = Boltzmann constant) shown in Fig. 9 revealed a straight line for each of the five peaks. The *E* and *s* were extracted from the slope of the lines and the intercept with the ordinate axis. These results are also shown in Table II. Overall, both analyzes yielded compatible *E* and *s* values with a general trend of finding larger differences among the values determined by the different methods for the high-temperature glow peaks, particularly peaks III and V.

Figure 10 presents a series of glow curves obtained after different times posterior to irradiation, up to 48 hrs. It is clear that peak I was unstable at room temperature, as already reported by the authors in [16]. The intensity of peak I continuously decreased for longer times after irradiation and was nearly extinguished after 1 hr. Further analysis of the TL signal fading was carried out by means of best fitting analysis using the GlowFit software. All the glow curves were fitted using the

same fixed set of values of *E* and *s* for each peak according to initial value at t = 0s. Fig. 11 shows the peak intensity and area of each peak as a function of the time after irradiation normalized to the respective intensities from the glow curve obtained after irradiation. 48 hrs post irradiation, the area of each peak was reduced (fading) by about 95% (peak I), 50% (peak II), 15% (peak III), 15% (peak IV), and 5% (peak V) of the initial value. This 5% of variation of peak V area could be an overestimation of the fading, as there might be contributions of fluctuations of the light detection efficiency of the TL equipment (typical values of 2% are expected), and of uncertainties of the glow-fitting method. The high stability of the TL signal to the higher temperature peaks over time suggests its potential use in the field of dosimetry. A further study with longer times after irradiation and a rigid control of the light detection efficiency could complement these findings.

In order for thermoluminescence to occur, it is necessary for a material to contain at least one trap and one recombination center. After the investigation of the traps through TL measurements presented above, we now focus on the investigation of the recombination centers by means of RL measurements. To the best of our knowledge, this is the first time that RL analysis of alexandrite was performed, with the RL spectra obtained as a function of the temperature being presented in Fig. 12. The RL spectrum obtained at room temperature is similar to the photoluminescence spectrum reported earlier [8], being composed by a narrow band centered at 1.82 eV superimposed to a broad band ranging from about 1.65 to 1.90 eV and centered at about 1.76 eV. The narrow band was assigned to the forbidden $^2E \rightarrow {}^4A_2$ transition of Cr^{3+} located in Al_2 sites [13, 16, 40-42]. The broad emission can be attributed to magnetically coupled Cr^{3+} - Cr^{3+} pairs and clusters, besides Fe^{3+} and Mn^{4+} impurities, commonly present in natural minerals [2, 43-47]. No additional emission was observed

at higher energies, as shown in the inset of Fig. 12. The evolution of the RL spectra as a function of temperature yielded insight into the thermal quenching of the luminescence centers. Both bands decreased in intensity and shifted to lower energies with increasing temperature. It is expected to reduce the emission of the R-lines due to competition between phonons and photons from the excited vibrionic states [48]. This is mainly due to the decrease in fluorescence life being stronger than increase in the effective cross section of the emission at increased temperatures [49]. Thermal quenching of these bands was further investigated by means of the following procedure: RL spectrum integration from 1.65 to 1.90 eV, visual determination of a baseline for the narrow band to compensate for its superposition onto the broad band, and subtraction of the area of the narrow band from the total area obtained previously. This way, the behavior of the integral intensity of each of the two bands was determined as a function of the temperature as shown in Fig. 13. These results revealed that the total RL integrated intensity decreased linearly with the temperature, while thermal quenching occurred at different rates for each band. Importantly, the Cr^{3+} in Al_2 sites is essentially thermally quenched around 475 K. Above this temperature, RL emission is dominated possibly by Cr^{3+} - Cr^{3+} pairs and clusters, Fe^{3+} and Mn^{4+} centers suggesting that the recombination center of TL peaks IV and V is predominantly related to these centers.

CONCLUSIONS

To the best of our knowledge, this is the first in-depth investigation of TL and RL of natural alexandrite. As expected, in addition to the main mineral phase alexandrite, the sample presented other mineral phases. More importantly, it also presented Cr^{3+} and Fe^{3+} as impurities. The T_m-T_{stop} analysis confirmed the presence of five peaks at 355, 405, 435, 530 and 580 K (β = 1 K/s) that, together with the analysis

based on the T_m as a function of dose method, were all demonstrated to exhibit a first-order kinetics TL mechanism. Also, we showed that the TL signal of all the peaks varied linearly with the beta irradiation dose from 1 to 10 Gy. The TL fading analysis showed that peak I is unstable at room temperature, and that the more intense peaks IV and V suffered a small reduction within two days after irradiation at room temperature. The values of the trap depth energy E and frequency factor s of all five TL peaks were determined by a combination of methods, variable heating rate and glow curve fitting, with both analyzes yielding compatible results. RL measurements as a function of the temperature revealed the presence of two recombination centers related to Cr^{3+}, Mn^{4+} and Fe^{3+} ions. In summary, based on the results above, alexandrite has shown to be a promising mineral for dosimetry, especially at high irradiation doses.

ACKNOWLEDGMENTS

N.M. Trindade received funding from the São Paulo Research Foundation (FAPESP), Grant #2017/11663-1. The authors are grateful to Nacional Council for Scientific and Technological Development (CNPq - Brazil), Grant #307375/2015-3. This material is based upon work supported by the National Science Foundation under Grant #1653016.

REFERENCES

[1] M. Rossi, M. Dell'Aglio, A. De Giacomo, R. Gaudiuso, G.S. Senesi, O. De Pascale, F. Capitelli, F. Nestola, M.R. Ghiara, Multi-methodological investigation of kunzite, hiddenite, alexandrite, elbaite and topaz, based on laser-induced breakdown spectroscopy and conventional analytical techniques for supporting mineralogical characterization, Physics and Chemistry of Minerals, 41 (2014) 127-140.

[2] M. Gafta, R. Reisfeld, G. Panckzer, Modern Luminescence Spectroscopy of Minerals and Materials, Springer Berlin, Heidelberg, New York, 2005.

[3] K. Kanchiang, A. Bootchanont, J. Witthayarat, S. Pramchu, P. Thanasuthipitak, R. Yimnirun, X-ray absorption spectroscopy and density functional analysis of the Fe3+ distribution profile on Al sites in a chrysoberyl crystal, BeAl2O4:Fe3+, Journal of Applied Crystallography, 49 (2016) 385-388.

[4] E.F. Farrel, J.H. Fang, H.P. Newhan, Refinement of the Chrysoberyl Structure., American Mineralogist, 48 (1963) 804-810.

[5] M.K. Rabadanov, A.P. Dudka, Comparative Structural Study of Al_2BeO_4 and $Al_2BeO_4:Cr^{3+}$. , Inorganic Materials, 33 (1997) 48-51.

[6] V.Y. Ivanov, V.A. Pustovarov, E.S. Shlygin, A.V. Korotaev, A.V. Kruzhalov, Electronic excitations in BeAl2O4, Be2SiO4, and Be3Al2Si6O18 crystals, Physics of the Solid State, 47 (2005) 466-473.

[7] R.M.F. Scalvi, M.S. Li, L.V.A. Scalvi, Thermal annealing-induced electric dipole relaxation in natural alexandrite, Physics and Chemistry of Minerals, 31 (2005) 733-737.

[8] K.L. Schepler, Fluorescence of inversion site Cr3+ ions in alexandrite, Journal of Applied Physics, 56 (1984) 1314-1318.

[9] R.M.F. Scalvi, L. de Oliveira Ruggiero, M. Siu Li, Influence of annealing on X-ray diffraction of natural alexandrite, Powder Diffraction, 17 (2002) 135-138.

[10] S.-U. Weber, M. Grodzicki, W. Lottermoser, G.J. Redhammer, G. Tippelt, J. Ponahlo, G. Amthauer, 57Fe Mössbauer spectroscopy, X-ray single-crystal diffractometry, and electronic structure calculations on natural alexandrite, Physics and Chemistry of Minerals, 34 (2007) 507-515.

[11] D.A. Vinnik, D.A. Zherebtsov, S.A. Archugov, M. Bischoff, R. Niewa, Crystal Growth and Characterization of Alexandrite, Crystal Growth & Design, 12 (2012) 3954-3956.

[12] B.K. Sevast'yanov, Excited-state absorption spectroscopy of crystals doped with Cr3+, Ti3+, and Nd3+ ions. Review, Crystallography Reports, 48 (2003) 989-1011.

[13] N. Ollier, Y. Fuchs, O. Cavani, A.H. Horn, S. Rossano, Influence of impurities on Cr3+ luminescence properties in Brazilian emerald and alexandrite, European Journal of Mineralogy, 27 (2015) 783-792.

[14] D.P. Groppo, L.V.E. Caldas, Luminescent response from BeO exposed to alpha, beta and X radiations, Radiation Measurements, 71 (2014) 81-85.

[15] E.G. Yukihara, S.W.S. Mckeever, Optically Stimulated Luminescence: Fundamentals and Applications, UK: John Wiley and Sons, West Sussex, 2011.

[16] N.M. Trindade, H. Kahn, E.M. Yoshimura, Thermoluminescence of natural BeAl2O4:Cr3+ Brazilian mineral: Preliminary studies, Journal of Luminescence, 195 (2018) 356-361.

[17] S.W.S. McKeever, Thermoluminescence of Solids, Cambridge University Press, Cambridge, 1985.

[18] J.M. Kalita, G. Wary, Thermoluminescence properties of minerals and their application, LAP LAMBERT Academic Publishing, Saarbrucken, Germany, 2016.

[19] A. Chruścińska, A. Szramowski, Thermally modulated optically stimulated luminescence (TM-OSL) of quartz, Journal of Luminescence, 195 (2018) 435-440.

[20] I.K. Bailiff, V.F. Stepanenko, H.Y. Goksu, L. Bøtter-Jensen, L. Brodski, V. Chumak, V. Correcher, A. Delgado, V. Golikov, H. Jungner, L.G. Khamidova, T.V. Kolizshenkov, I. Likhtarev, R. Meckbach, S.A. Petrov, S. Sholom, Comparison of retrospective luminescence dosimetry with computational modeling in two highly contaminated settlements downwind of the Chernobyl NPP, Health Physics, 86 (2004) 25-41.

[21] P. Beneitez, V. Correcher, A. Millán, T. Calderon, Thermoluminescence analysis for testing the irradiation of spices, Journal of Radioanalytical and Nuclear Chemistry, 185 (1994) 401-410.

[22] V. Correcher, J. Garcia-Guinea, L. Sanchez-Muñoz, T. Rivera, Luminescence characterization of a sodium-rich feldspar, Radiation Effects & Defects in Solids, 162 (2007) 709-714.

[23] R. Kibar, J. Garcia-Guinea, A. Çetin, S. Selvi, T. Karal, N. Can, Luminescent, optical and color properties of natural rose quartz, Radiation Measurements, 42 (2007) 1610-1617.

[24] F. Preusser, M.L. Chithambo, T. Götte, M. Martini, K. Ramseyer, E.J. Sendezera, G.J. Susino, A.G. Wintle, Quartz as a natural luminescence dosimeter, Earth-Science Reviews, 97 (2009) 184-214.

[25] F.O. Ogundare, M.L. Chithambo, Thermoluminescence kinetic analysis of quartz with a glow peak that shifts in an unusual manner with irradiation dose, Journal of Physics D: Applied Physics, 40 (2007) 247-253.

[26] W.F. Hornyak, R. Chen, A. Franklin, Thermoluminescence characteristics of the 375 °C electron trap in quartz, Physical Review B, 46 (1992) 8036-8049.

[27] J.F. de Lima, M.E.G. Valerio, E. Okuno, Thermally assisted tunneling: An alternative model for the thermoluminescence process in calcite, Physical Review B, 64 (2001) 014105.

[28] Y.A. Abdel-Razek, Thermoluminescence dosimetry using natural calcite, Journal of Taibah University for Science, 10 (2016) 286-295.

[29] A. Pandya, S.G. Vaijapurkar, P.K. Bhatnagar, Radiation dosimetry by potassium feldspar, Bulletin of Materials Science, 23 (2000) 155-158.

[30] V. Pagonis, M.L. Chithambo, R. Chen, A. Chruścińska, M. Fasoli, S.H. Li, M. Martini, K. Ramseyer, Thermal dependence of luminescence lifetimes and radioluminescence in quartz, Journal of Luminescence, 145 (2014) 38-48.

[31] P.N. Yaravoi, V.Y. Medvedev, G.V. Bukin, L.A. Ivanova, A.A. Mikhalenko, Radiative Creation of Color Centers in Alexandrite Crystals, Opt. Spectrosc., 71 (1991) 447-449.

[32] G. M. Ferraz, S. Watanabe, S. O. Souza, R. M. F. Scalvi, TL, EPR and Optical Absorption Studies on Natural Alexandrite Compared to Natural Chrysoberyl, Radiation Protection Dosimetry, 100 (2002) 471-474.

[33] V. Pagonis, G. Kitis, C. Furetta, Numerical and Practical Exercises in Thermoluminescence, 1 ed., Springer-Verlag New York, 2006.

[34] C. Furetta, Handbook of Thermoluminescence, World Scientific, 2003.

[35] M. Puchalska, P. Bilski, GlowFit—a new tool for thermoluminescence glow-curve deconvolution, Radiation Measurements, 41 (2006) 659-664.

[36] J.T. Randall, M.H.F. Wilkins, Phosphorescence and electron traps - I. The study of trap distributions, Proceedings of the Royal Society of London. Series A. Mathematical and Physical Sciences, 184 (1945) 365-389.

[37] N.M. Trindade, R.M.F. Scalvi, L.V.d.A. Scalvi, Cr+3 Distribution in Al1 and Al2 Sites of Alexandrite (BeAl2O4: Cr3+) Induced by Annealing, Investigated by Optical Spectroscopy, Energy and Power Engineering, 2 (2010) 18-24.

[38] N.M. Trindade, A.R. Blak, E.M. Yoshimura, L.V.d.A. Scalvi, R.M.F. Scalvi, Photo-Induced Thermally Stimulated Depolarization Current (TSDC) in Natural and Synthetic Alexandrite (BeAl2O3: Cr3+), Materials Sciences and Applications, 7 (2016) 881-894.

[39] J.M. Kalita, M.L. Chithambo, Comprehensive kinetic analysis of thermoluminescence peaks of α-Al2O3:C,Mg, Journal of Luminescence, 185 (2017) 72-82.

[40] N.M. Trindade, A.S. Tabata, R.M.F. Scalvi, L.V.d.A. Scalvi, Temperature Dependent Luminescence Spectra of Synthetic and Natural Alexandrite, Materials Sciences and Applications, 2 (2011) 284-287.

[41] R.C. Powell, L. Xi, X. Gang, G.J. Quarles, J.C. Walling, Spectroscopic properties of alexandrite crystals, Physical Review B, 32 (1985) 2788-2797.

[42] A.B. Suchocki, G.D. Gilliland, R.C. Powell, J.M. Bowen, J.C. Walling, Spectroscopic properties of alexandrite crystals II, Journal of Luminescence, 37 (1987) 29-37.

[43] V. Lisitsyn, E. Polisadova, D. Valiev, Pulsed cathodoluminescence of calcite crystals of various origins, Inorganic Materials, 48 (2012) 738-744.

[44] M. Kaiheriman, A. Maimaitinaisier, A. Rehiman, S. Aierken, Photoluminescence properties of green and red luminescence from natural and heat-treated sodalite, Physics and Chemistry of Minerals, 41 (2014) 227-235.

[45] N.R.J. Poolton, L. Bøtter-Jensen, O. Johnsen, On the relationship between luminescence excitation spectra and feldspar mineralogy, Radiation Measurements, 26 (1996) 93-101.

[46] M. Gaft, G. Panczer, L. Nagli, H. Yeates, Laser-induced time-resolved luminescence of tugtupite, sodalite and hackmanite, Physics and Chemistry of Minerals, 36 (2009) 127-141.

[47] V. Correcher, J. Garcia-Guinea, Cathodo- and photoluminescence emission of a natural Mg-Cr carbonate layered double hydroxide, Applied Clay Science, 161 (2018) 127-131.

[48] D. Pugh-Thomas, B.M. Walsh, M.C. Gupta, Spectroscopy of BeAl2O4:Cr3+ with application to high-temperature sensing, Appl. Opt., 49 (2010) 2891-2897.

[49] I. Yorulmaz, E. Beyatli, A. Kurt, A. Sennaroglu, U. Demirbas, Efficient and low-threshold Alexandrite laser pumped by a single-mode diode, Opt. Mater. Express, 4 (2014) 776-789.

TABLE CAPTIONS

Table I - Normalized EDS results of natural alexandrite (sample I) according to stochiometric proportions in wt.%, except for mica. The results for the alexandrite and mica phases correspond to the average of 39 and 9 different point measurements, respectively.

Table I

Alexandrite	**BeO**		**Al_2O_3**		**Cr_2O_3**		**Fe_2O_3**				**Total**
	19.46		77.09		1.85		1.60				100.00
Mica	**MgO**		**Al_2O_3**	**Cr_2O_3**	**Fe_2O_3**		**SiO_2**	**MnO**			**Total**
	19.84		21.56	0.55	17.17		26.6	0.72			86.44
Allanite	**MgO**	**Al_2O_3**	**Fe_2O_3**	**SiO_2**	**MnO**	**CaO**	**Cl**	**La_2O_3**	**Ce_2O_3**	**Nd_2O_3**	**Total**
	0.62	23.74	8.05	35.23	1.38	16.86	0.37	4.63	7.31	1.81	100.00
Apatite	**CaO**		**SrO**	**P_2O_5**		**F**					**Total**
	52.90		1.20	42.30		3.60					100.00
Fluorite	**CaO**		**F**								**Total**
	51.30		48.70								100.00

Table II - Trap depth energy and frequency factor values of TL peaks I to V obtained by different methods. See text for details.

Table II

	Depth trap energy (eV)	
Peak	T_m - dose method	Variable heating rate method
I	0.73 ± 0.06	0.66 ± 0.03
II	0.77 ± 0.02	0.78 ± 0.03
III	0.69 ± 0.02	0.91 ± 0.03
IV	1.07 ± 0.02	1.16 ± 0.04
V	1.04 ± 0.01	1.29 ± 0.07
	Frequency factor s (s^{-1})	
Peak	T_m - dose method	variable heating rate method
I	(5.53 ± 5.26) x 10^9	(1.76 ± 0.16) x 10^8
II	(2.86 ± 2.58) x 10^8	(2.95 ± 0.27) x 10^8
III	(3.30 ± 1.69) x 10^6	(1.18 ± 0.09) x 10^9
IV	(1.18 ± 0.41) x 10^9	(7.22 ± 0.60) x 10^8
V	(3.86 ± 0.86) x 10^7	(6.87 ± 0.42) x 10^9

FIGURE CAPTIONS

Figure 1 - (a) visual aspect of the fragments of sample I; (b) BSE image of the fragments of sample I; BSE image of the fragment of sample I with the highest fraction of alexandrite at (c) low and (d) high magnification.

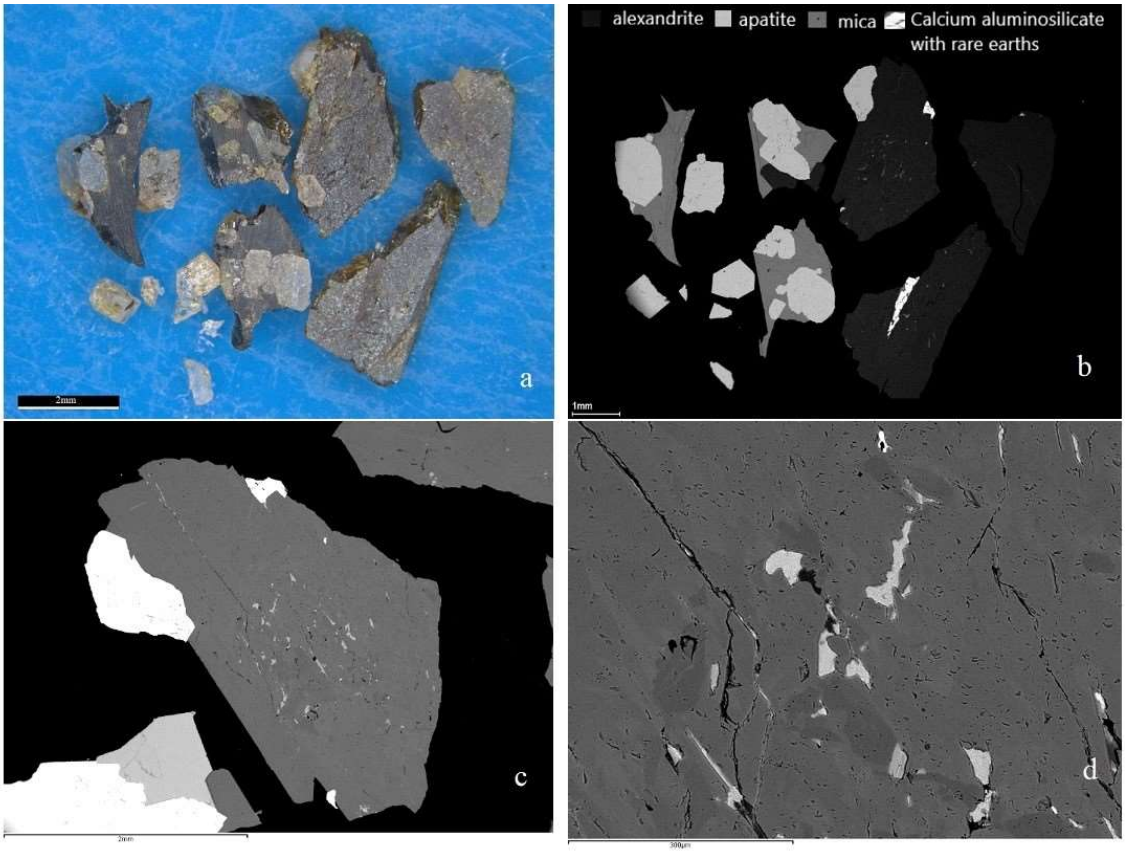

Figure 2 - TL glow curve of natural alexandrite in semi-log scale obtained at 1 K/s heating rate after a 1 Gy irradiation dose where the five TL peaks are identified.

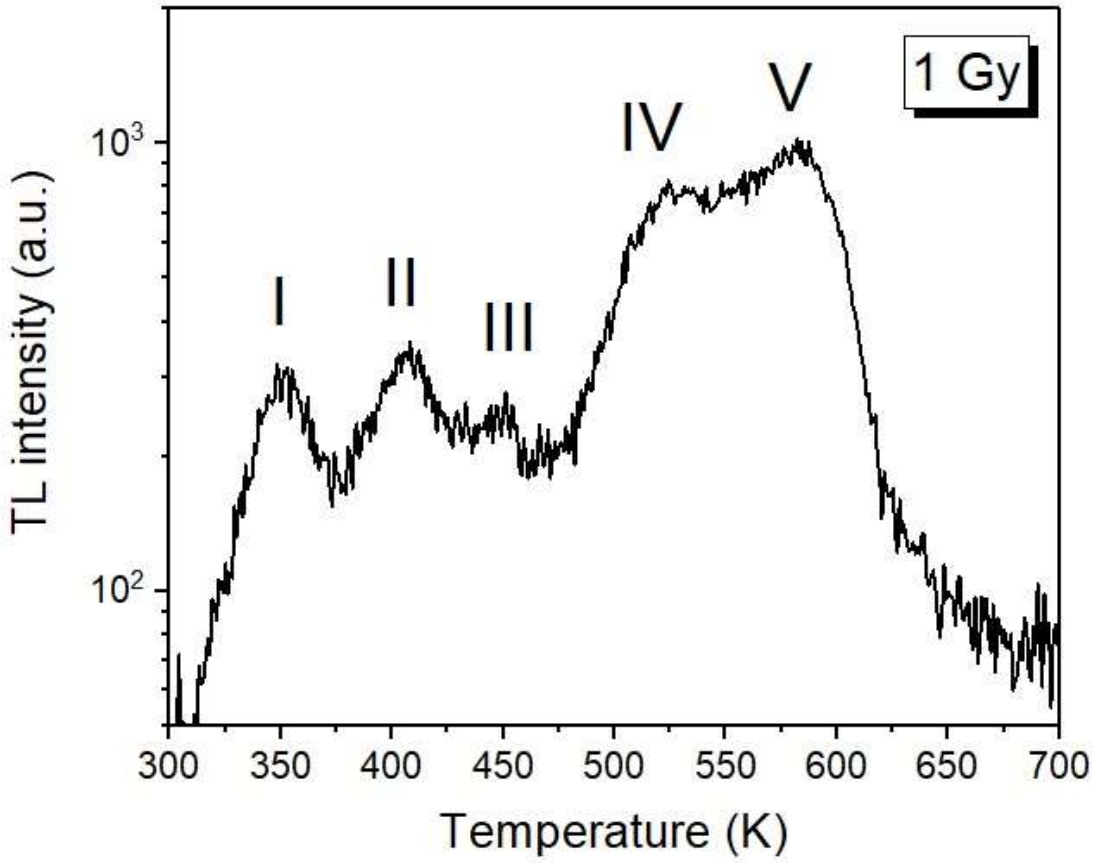

Figure 3 - T_m-T_{stop} curve from natural alexandrite where five TL peaks are identified.

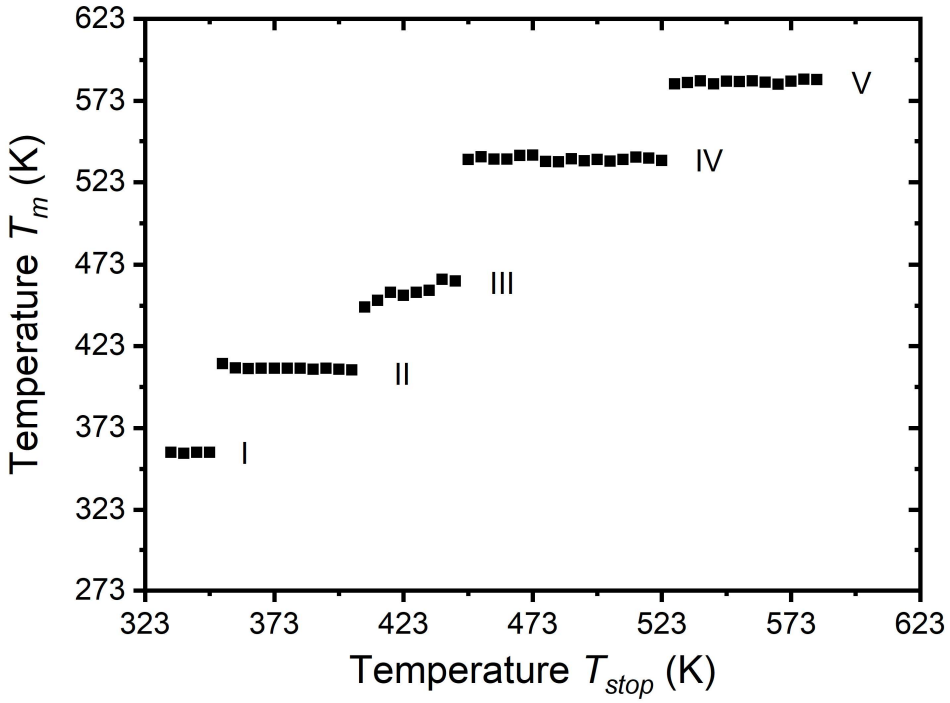

Figure 4 - TL glow curve of natural alexandrite as a function of the beta irradiation dose (1 K/s). The inset shows the position of each peak obtained by visual inspection and through analysis using the GlowFit software.

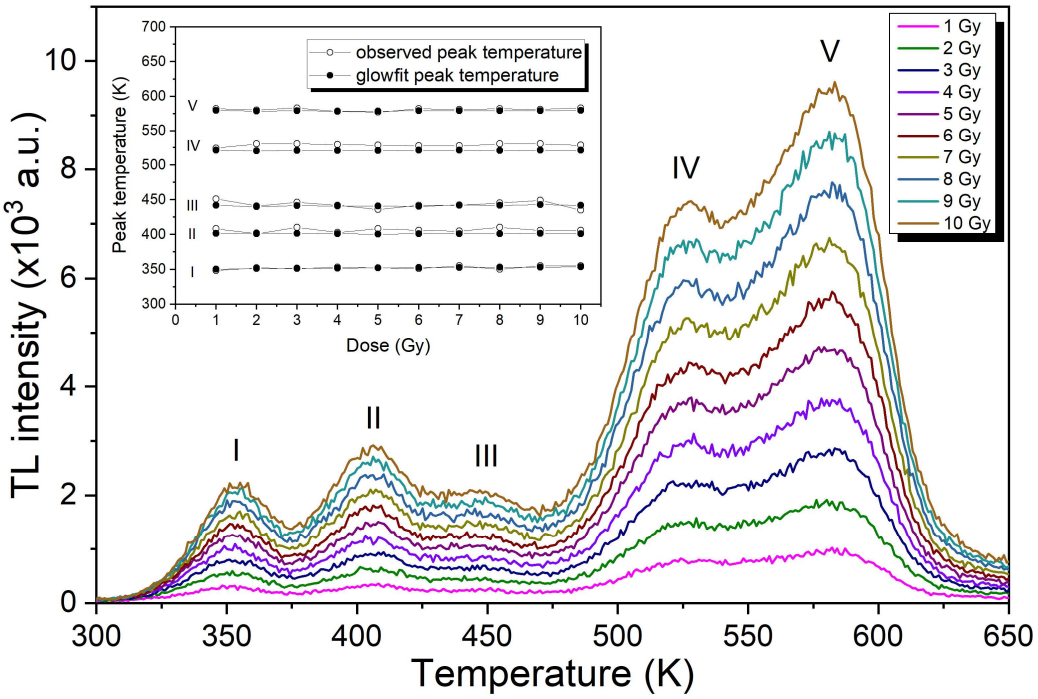

Figure 5 - Best fitting of TL glow curves obtained with different irradiation doses, from 1 to 10 Gy.

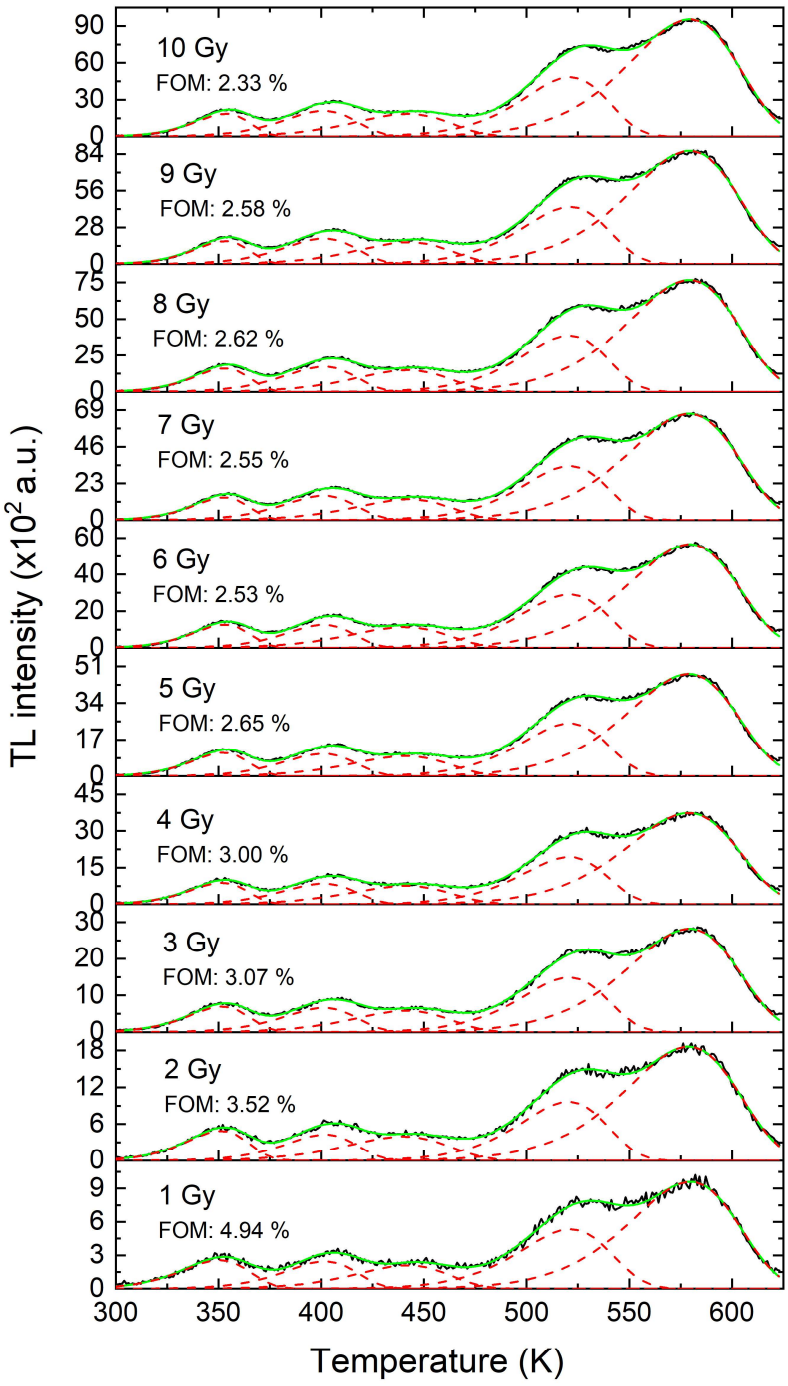

Figure 6 - (a) Peak intensity and (b) integrated intensity (area) of the five individual bands used in the GlowFit best fit analysis of glow curves as a function of the irradiation dose.

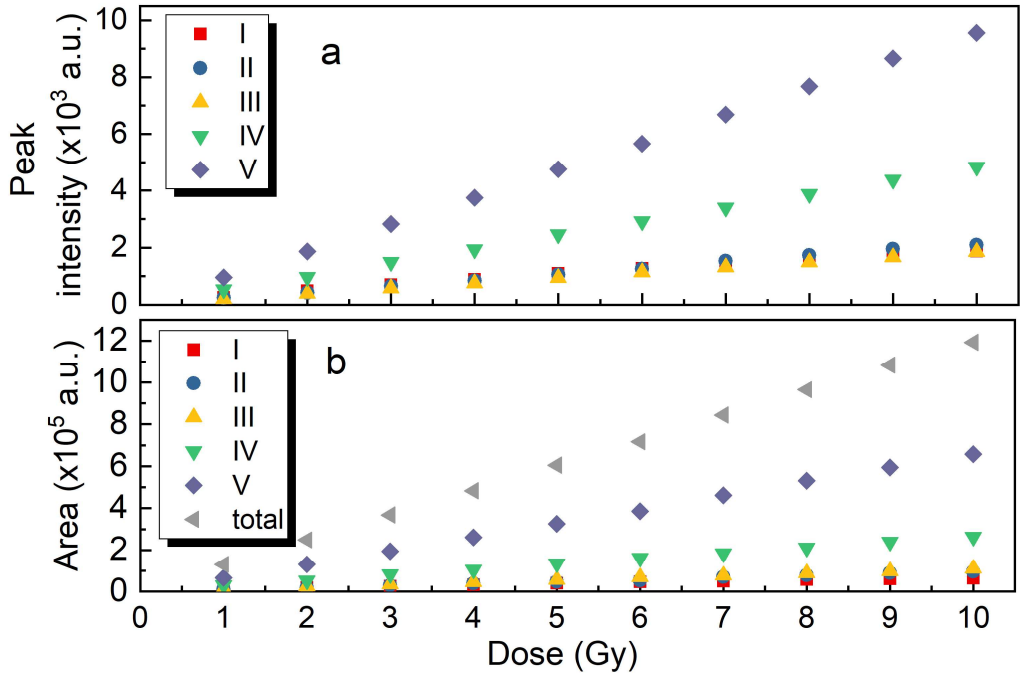

Figure 7 - Average depth trap energy values obtained through the GlowFit best fit analysis of TL glow curves as a function of the irradiation dose. The dashed lines mark the average value and the dotted lines the limits of the standard deviation, with the exception of peak I.

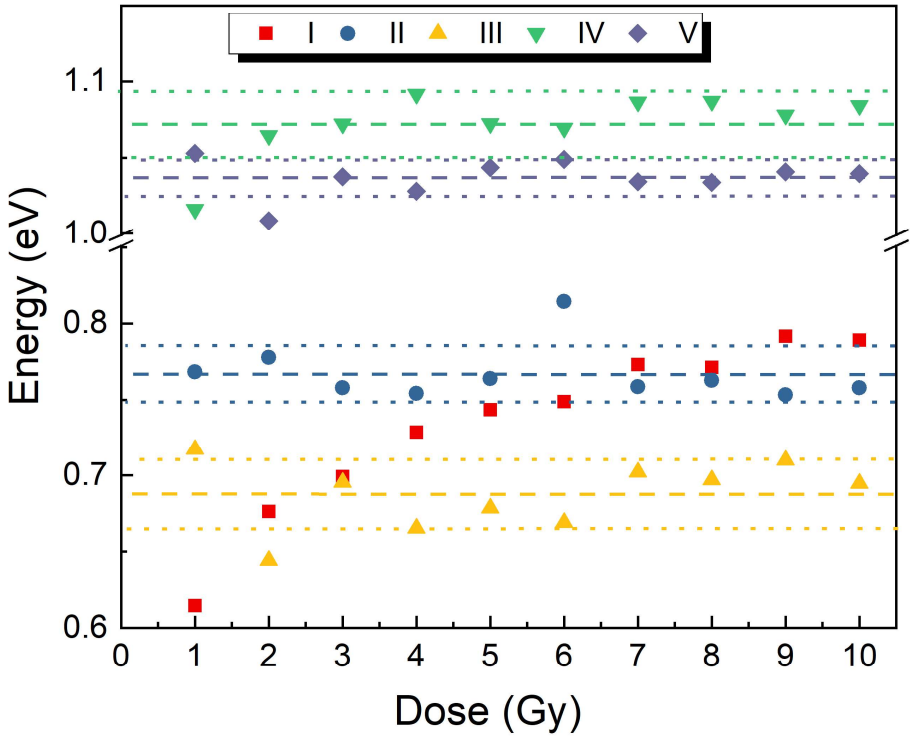

Figure 8 - TL glow curves obtained at different heating rates after a beta irradiated dose of 1 Gy.

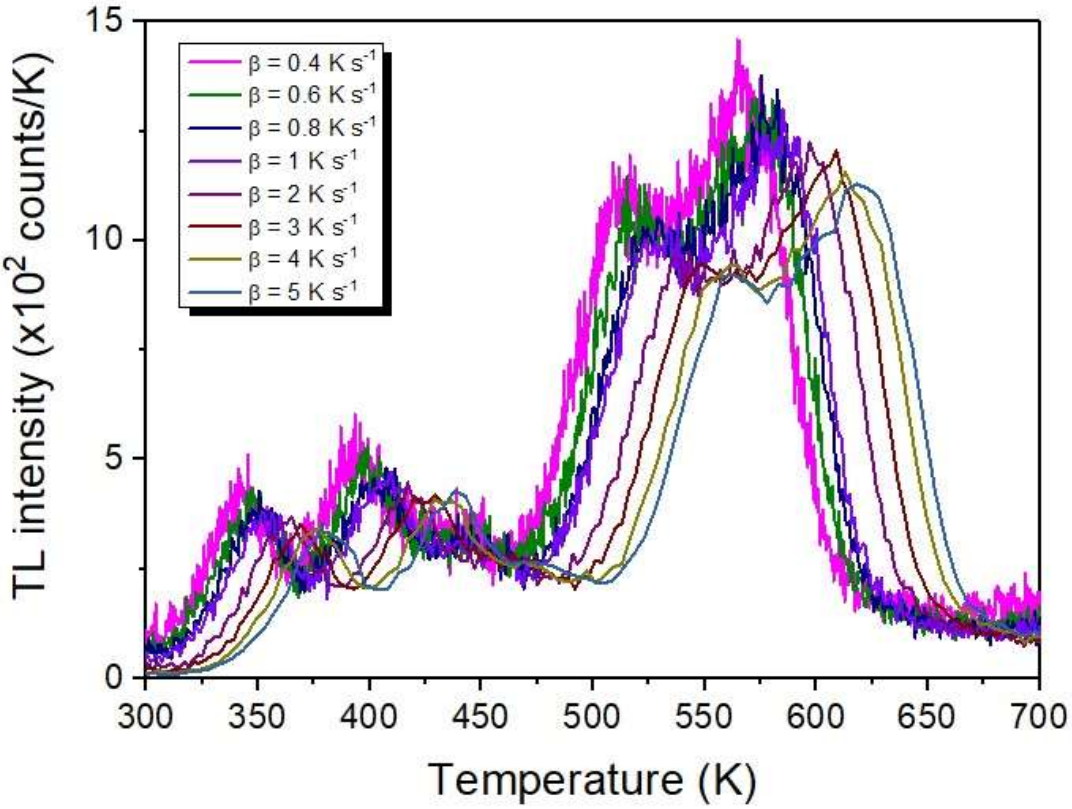

Figure 9 - Plot of $ln(T_m^2/\beta)$ against $1/kT_m$ of TL peaks I to V, according to the variable heating rate method. The red lines correspond to linear best fits.

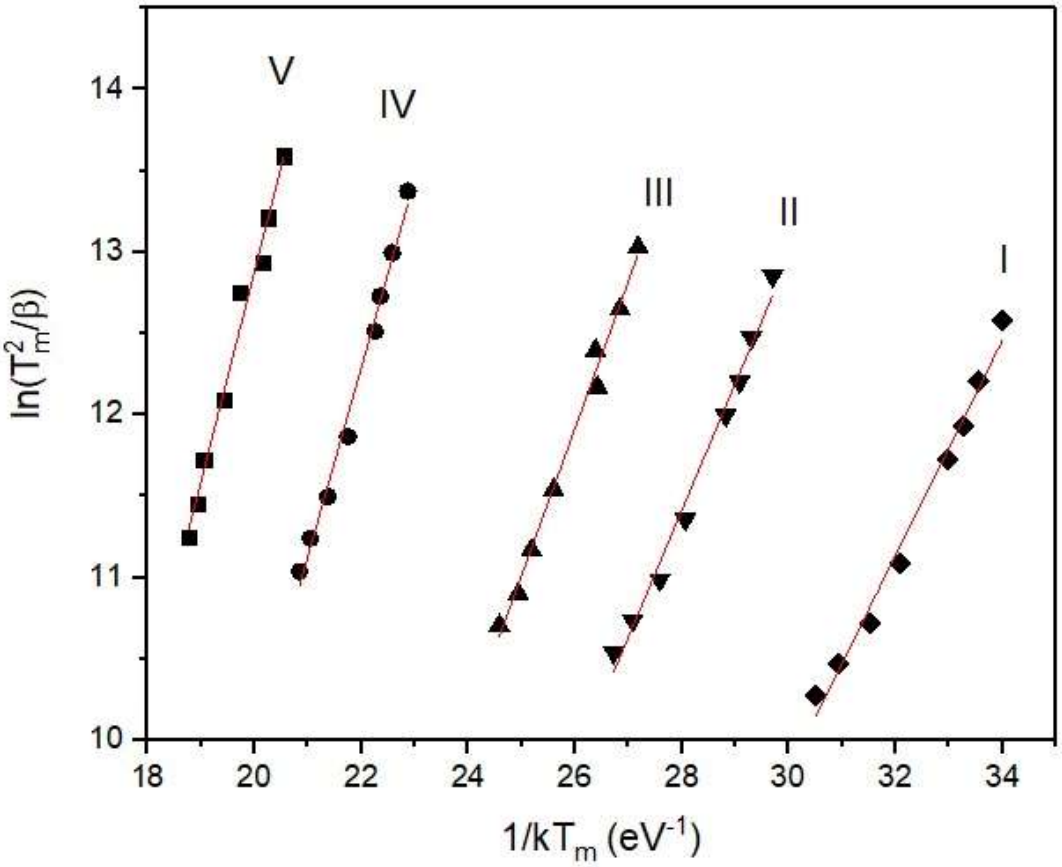

Figure 10 - TL glow curves (1 K/s; 1 Gy) obtained after different times after irradiation up to 48 hrs.

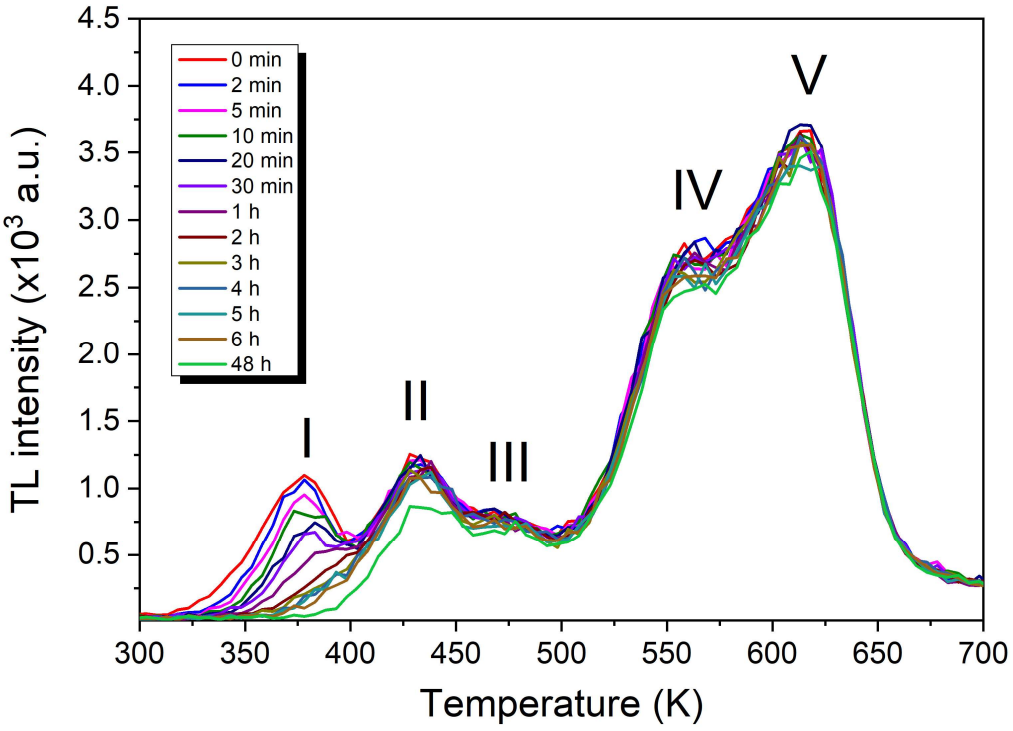

Figure 11 - (a) Normalized peak intensity and (b) normalized area of the five individual TL peaks obtained as a function of time after irradiation. The results were normalized to the respective values obtained immediately after irradiation.

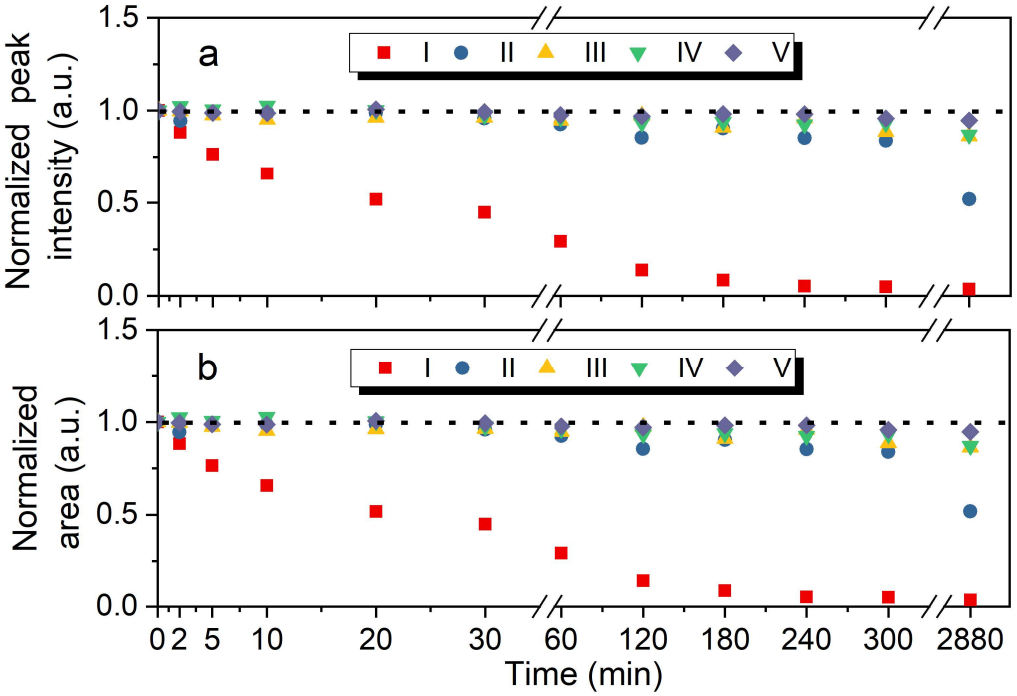

Figure 12 - RL spectra of the natural alexandrite as a function of temperature. The inset presents the spectra at higher photon energies, up to 4 eV; the emission around 2 eV corresponds to the tail of the emission band shown in the main figure.

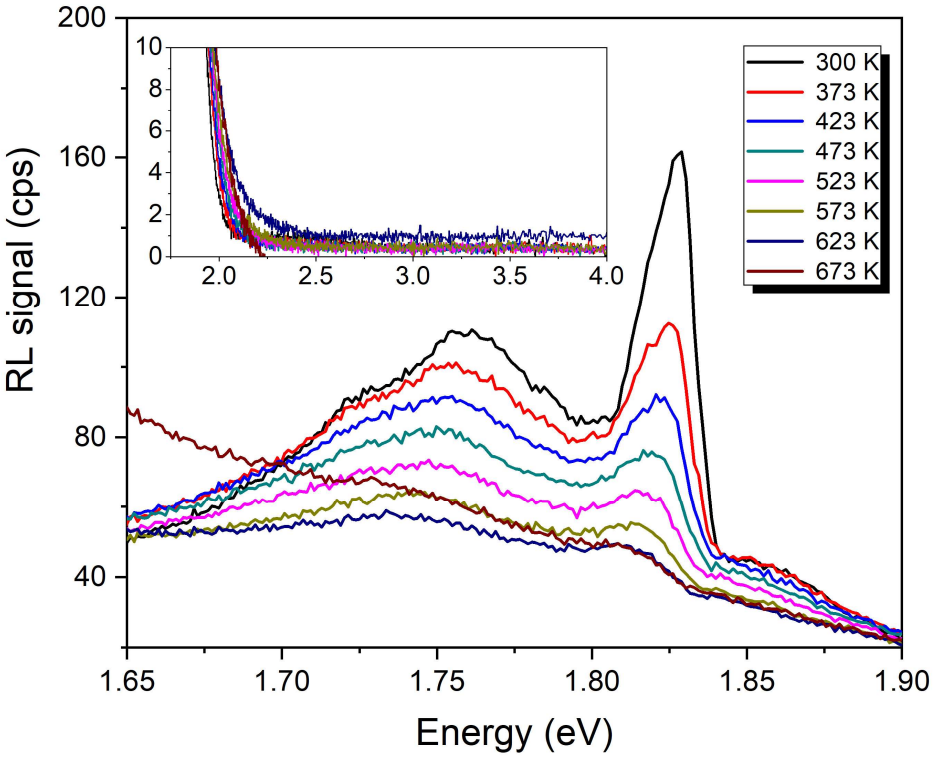

Figure 13 - Total RL integrated intensity (squares) and integrated intensity of the 1.76 eV (triangles) and 1.82 eV (circles) individual emission bands related to the impurities as a function of the temperature. The red line corresponds to the linear best fit of the total RL integrated intensity ($R^2 = 0.99$).